Dendrite to symmetry-broken dendrite transition in directional solidification of non-axially oriented crystals*

Xing Hui(邢 辉)[a)b)], Wang Jian-Yuan(王建元)[a)b)], Chen Chang-Le(陈长乐)[a)b)†], Jin Ke-Xin(金克新)[a)b)], and Du Li-Fei(杜立飞)[b)]

[a)] *Shaanxi Key Laboratory for Condensed Matter Structure and Properties, Northwestern Polytechnical University, Xi'an* 710129, *China*
[b)] *The Key Laboratory of Space Applied Physics and Chemistry, Northwestern Polytechnical University, Xi'an* 710072, *China*

(Received 1 April 2013; revised manuscript received 2 September 2013; published online 24 January 2014)

In this paper, the morphological transition from dendrite to symmetry-broken dendrite is investigated in the directional solidification of non-axially-oriented crystals using a quantitative phase-field model. The effects of pulling velocity and crystal orientation on the morphological transition are investigated. The results indicate the orientation dependence of the symmetry-broken double dendrites. A dendrite to symmetry-broken dendrite transition is found by varying the pulling velocity at different crystal orientations and the symmetry-broken multiple dendrites emerge as a transition state for the symmetry-broken double dendrites. The state region during the transition can be well characterized through the variations of the characteristic angle and the average primary dendritic spacing.

Keywords: directional solidification, phase-field simulations, symmetry broken

PACS: 81.30.Fb, 68.70.+w **DOI:** 10.1088/1674-1056/23/3/038104

1. Introduction

Solidification microstructure pattern formation is a widely investigated subject in nonequilibrium and nonlinear statistical physics.[1,2] Dendrite is the most frequently formed morphology of non-faceted crystals in solidification processing, where the anisotropy of the surface tension clearly plays an important role in stabilizing the dendritic tip with the dendrite growing into a free space.[3] In directional solidification, the sample is pulled through a linear temperature gradient at a constant pulling velocity, which gives rise to a variety of interfacial patterns.[4,5] The temperature gradient and the pulling velocity are two control parameters in the directional solidification. The most basic microstructure pattern is a periodic array of cells or dendrites that forms when the pulling velocity exceeds a critical velocity which is presented by the Mullins–Sekerka instability.[6] In the last decades, studies in experiments and simulations show that possible steady-state patterns forming in the directional solidification are much richer than that ever anticipated. Symmetry-broken (SB) double cells (doublets) in directional solidification, i.e., two asymmetrical cells which are mirror images of each other with a deep groove between them, were first observed in experiments by Jamgotchian *et al.*[7] The existence of SB multiple cells (triplets or multiplets) was also noted in their work. Following their work, a number of theories, simulations, and experiments[8–18] have probed the stability, characteristics, and formation of SB fingers. The simulations presented by Kopczynski *et al.*[8] revealed the existence of branches of SB double cells and higher-order multiple ones with narrow grooves. By imposing a periodic perturbation in phase-field simulations, Losert *et al.*[9] tested the stability of the SB double cells, and they found that the SB double cells only have a transient state without the imposed perturbation. Akamatsu *et al.*[10] observed experimentally the SB double dendrites in a thin-film directional solidification in a velocity range higher than that for the cellular case. Both types of SB double fingers (cells and dendrites) have the same symmetry but different branch origins. Hence, they should be treated as a separated morphological class. As shown in Ref. [8], the SB double cells, the one branch of the series of SB multiple cells, emerge when the pulling velocity is low. In contrast, the SB double dendrites emerge when the pulling velocity is high. They are possibly related to the morphologies of the doublon branch found by Ihle and Muller-Krumbhaar[12] and Singer *et al.*[13] although their studies are based on the dendritic solidification in a pure undercooled melt.

In the directional solidification of a non-axially-oriented crystal, the orientation of the crystal ($\langle 100 \rangle$ for ordinary face-centered cubic (fcc) and body-centered cubic (bcc) alloys) must be specified with respect to the axis of the thermal gradient which is also the axis of the pulling velocity. The angle between the orientation of the crystal and the axis of the thermal gradient can be defined as Θ_0. The most obvious characteristic of the actual crystal growth direction is that the growth direction rotates from the thermal gradient direction to the crystal

*Project supported by the National Natural Science Foundation of China (Grant Nos. 61078057 and 51172183), the National Natural Science Foundation of Shaanxi Province, China (Grant No. 2012JQ8013), the Aviation Foundation of China (Grant No. 2011ZF53065), and the NPU Foundation for Fundamental Research, China (Grant Nos. NPU-FFR-JC20110273 and JC201155).

†Corresponding author. E-mail: chenchl@nwpu.edu.cn

© 2014 Chinese Physical Society and IOP Publishing Ltd

orientation direction with the increase of the pulling velocity at a constant thermal gradient, which can only be attributed to the interfacial anisotropy.[19–21] Usually, the growth pattern strongly depends on the crystal orientation with respect to the solidification setup. A large variety of interfacial patterns hence emerge in the directional solidification of such non-axially-orientated crystals. Except for the pulling velocity and the thermal gradient, it is believed that the dendrite to SB dendrite transition depends sensitively on the sample thickness, crystal orientation, and possible solute segregation. Based on experimental results, Akamatsu *et al.*[9] provided schematic diagrams of growth patterns as a function of the orientation of the crystal and the pulling velocity, where the SB double dendrites appear at high pulling velocities. Utter *et al.*[22] found that the stable SB double dendrites break apart into unstable structures with the increase of the solute concentration in experiments. However, the precise mechanism of the dendrite to SB dendrite transition remains unclear. Therefore, understanding how the transition is controlled by the thermal gradient, pulling velocity, and crystalline orientation is crucial not only for carrying out experiments of directional solidification of real alloys and transparent alloys but also for predicting the microstructure evolution by numerical methods.

In this paper, we report phase-field simulations that isolate the effects of the pulling velocity and the crystalline orientation on the dendrite to symmetry-broken dendrite transition and the stability of growth patterns. A full quantitative phase-field model[23] is used to carry out our two-dimensional simulations. Wang *et al.*[24,25] have discussed the non-equilibrium effects of this quantitative phase-field model and the initial instability with different surface tension anisotropies. With different crystalline orientations, a morphological transition from dendrite (or cell) to symmetry-broken dendrites, including double or even higher-order multiple ones, is found as the pulling velocity is increased. The state region during the transition can be shown to be well characterized through the variations of the characteristic angle Θ and the average primary dendritic spacing λ^*. According to the results of our phase-field simulations, a detailed transition map has been plotted.

2. Model and method

We first consider the directional solidification of a dilute binary alloy with straight solidus and liquidus lines of slopes m/k and m, respectively. The concentrations of solute at the solid side and the liquid side of the solid–liquid interfaces yields the partition relation $c_\mathrm{s} = kc_\mathrm{l}$, where k is the partition coefficient. Because the diffusion of solute in the solid is typically several orders of magnitude lower than that in the liquid, the diffusion in the solid can be neglected, i.e., one-sided model. Since the latent heat production is neglected, the so-called frozen temperature approximation is adopted for the directional solidification issues, yielding

$$T = T_0 + G(z - V_\mathrm{p}t), \tag{1}$$

where T_0 is a reference temperature, the temperature gradient G is aligned with the z direction, and the sample is pulled with a constant pulling velocity V_p. Furthermore, the convection in the liquid is also neglected. For the surface tension anisotropy, a four-fold anisotropy is implemented here, where the anisotropy function can be expressed as

$$A(\psi) = 1 + \varepsilon \cos 4(\psi - \Theta_0), \tag{2}$$

where ε is the anisotropic intensity of the surface tension, ψ is the angle between the direction normal to the interface and the thermal gradient direction, and Θ_0 is the misorientation angle. With the above assumptions, the sharp-interface equations for the directional solidification of a dilute alloy are

$$\partial_t c = D_\mathrm{l}\nabla^2 c, \tag{3}$$

$$c_\mathrm{l}(1-k)\boldsymbol{V}_n = -D_\mathrm{l}\partial c/\partial \boldsymbol{n}|_\mathrm{l}, \tag{4}$$

$$c_\mathrm{l}/c_\mathrm{l}^0 = 1 - (1-k)d_0\kappa\left[A(\psi) + \partial_2 A(\psi)/\partial\psi^2\right] - (1-k)\left(z - V_\mathrm{p}t\right)/l_\mathrm{T} - (1-k)\beta V_n, \tag{5}$$

where c_∞ is the far-field solute concentration, $c_\mathrm{l}^0 = c_\infty/k$ is the concentration at the liquid side of the interface, D_l is the solute diffusivity in the liquid phase, l_T is the thermal length, k is the partition coefficient, m is the liquidus slope, $\boldsymbol{V}_n$ is the interface velocity, κ is the curvature of the interface, $d_0 = \Gamma/\Delta T_0$ is the capillary length, Γ is the Gibbs–Thomson coefficient, $\Delta T_0 = |m|(1-k)c_\mathrm{l}^0$ is the freezing range, $l_\mathrm{T} = |m|c_\infty(1-k)/(kG)$ is the thermal length, $l_\mathrm{D} = D_\mathrm{l}/V_\mathrm{p}$ is the solute diffusion length, and $\beta = 1/(\mu_\mathrm{k}\Delta T_0)$ is the kinetic coefficient. The characteristic lengths of this problem are d_0 and l_D.

The phase-field model of dilute binary alloy directional solidification with the anti-trapping current proposed by Echebarria *et al.*[24] to model the limit of local thermodynamic equilibrium at the solid–liquid interface is employed here. This model is the only fully quantitative phase-field model for directional solidification that allows for unequal solute diffusivities in the solid and liquid. The previous investigations demonstrate that this model allows for accurate and fully grid independent simulations of alloy solidification on the microstructure scale. With constant material properties, this model neglects the solute diffusion in the solid. It can reduce to the sharp-interface model in the thin interface limit when the kinetic effects are neglected. The thickness of the interface is chosen to be smaller than the dendritic tip radius but larger than the width of the real solid–liquid interface. In the phase-field model, ϕ, representing the phase field, takes on the values $\phi = 1$ in the bulk solid phase and $\phi = -1$ in

the bulk liquid phase. It goes smoothly within the interface region. The complete set of phase-field equations with crystalline anisotropy is given by

$$\begin{aligned}
&\tau(\psi)\left[1-(1-k)\frac{z-V_{\mathrm{p}}t}{l_{\mathrm{T}}}\right]\frac{\partial\phi}{\partial t}\\
&=\nabla\cdot\left[W^2(\psi)\nabla\phi\right]+\partial_x\left(|\nabla\phi|^2W(\psi)\frac{\partial W^2(\psi)}{\partial(\partial_x\phi)}\right)\\
&\quad+\partial_z\left(|\nabla\phi|^2W(\psi)\frac{\partial W^2(\psi)}{\partial(\partial_z\phi)}\right)\\
&\quad+\phi-\phi^3+\lambda\left(1-\phi^2\right)^2\left(U+\frac{z-V_{\mathrm{p}}t}{l_{\mathrm{T}}}\right), \qquad (6)\\
&\left[\frac{1+k}{2}-\frac{(1-k)\phi}{2}\right]\frac{\partial U}{\partial t}\\
&=\nabla\cdot\left[D\frac{1-\phi}{2}\nabla U+\frac{W}{2\sqrt{2}}\left[1+(1-k)U\right]\frac{\partial\phi}{\partial t}\frac{\nabla\phi}{|\nabla\phi|}\right]\\
&\quad+\frac{1}{2}\left[1+(1-k)U\right]\frac{\partial\phi}{\partial t}, \qquad (7)\\
&U=\left[(2kc/c_\infty)(1+k-(1-k)\phi)-1\right]/(1-k), \qquad (8)\\
&W(\psi)=W_0A(\psi), \qquad (9)\\
&\tau(\psi)=\tau_0A^2(\psi), \qquad (10)
\end{aligned}$$

where ψ is the angle between the direction normal to the interface and the horizontal axis, and U is the dimensionless solute concentration in the whole domain. The parameters of the interface thickness for the phase field are linked to the physical quantities by two relations $d_0=a_1W_0/\lambda$ and $\tau_0=a_2\lambda W_0^2/D_{\mathrm{l}}$, where the constants are $a_1=0.8839$ and $a_2=0.6267$. Here τ_0 and W_0, representing the relaxation time and a measure of the interface width, respectively, are used to non-dimensionalize Eqs. (6) and (7).

The dendrite to symmetry-broken dendrite transition simulations presented in the following are for the Al–3 wt.% Cu alloy. The physical properties of the alloy[1] are provided as follows: the liquid diffusion coefficient $D=3000\ \mu\mathrm{m}^2/\mathrm{s}$, the partition coefficient $k=0.14$, the Gibbs–Thomson coefficient $\Gamma=0.24\ \mathrm{K}\cdot\mu\mathrm{m}$, the slope of the liquidus line $m=-2.6\ \mathrm{K/wt.\%}$, and the chemical capillary length $d_0=5\times10^{-3}\ \mu\mathrm{m}$. The surface tension anisotropy intensity is $\varepsilon=0.01$ as shown in Ref. [26]. Equations (6) and (7) are solved by using the explicit finite difference method on a fixed grid. A schematic diagram of the computational domain used in the present directional solidification simulations is shown in figure 1(a). The bottom and the top boundaries are treated periodically to reduce the domain size, and no-flux boundary conditions are applied to the left and the right boundaries for both ϕ and U. The system size is 600×3000 with grid spacing $\Delta x/W=0.8$ and time step $\Delta t/\tau_0=0.008$. In the phase-field simulations, the thickness of the interface increases with the increase of the coupling constant λ. As discussed in Refs. [23] and [27], $\lambda=10$ can be used for the independent results of the interface width. We simulate the directional solidification with $\boldsymbol{V}_{\mathrm{p}}$ oriented along the z axis and the surface tension anisotropy oriented in the $\langle100\rangle$ direction while the crystal grows in the real direction $\boldsymbol{V}_{\mathrm{g}}$. It is well known that the angle between the real growth direction $\boldsymbol{V}_{\mathrm{g}}$ and the z axis is Θ rather than Θ_0. The initial value for the dimensionless concentration U is taken as -1 ($C=C_\infty$). Simulations start from a planar solidification front applied by a sinusoidal perturbation

$$\delta=\delta_0\sin\left(\lambda_{\mathrm{f}}x\right), \qquad (11)$$

where δ_0 is the amplitude of this sinusoidal perturbation, and λ_{f} is the wavelength. In the simulations, we use a very small amplitude (δ_0 is $2\Delta x/W$) to provide the initial perturbation to the solidification front. The wavelength $\lambda_{\mathrm{f}}=13.5\ \mu\mathrm{m}$ is used here. Note that the sinusoidal perturbation can be introduced in experiments by using a perturbation technique reported by Losert *et al.*[9] To study the effect of the velocity on the transition, the thermal gradient $G=0.07\ \mathrm{K}/\mu\mathrm{m}$ is fixed for all simulations and V_{p} is examined from 500 μm/s to 16000 μm/s, while Θ_0 is varied from 15° to 40°. For $\Theta_0=45°$, a transition of growth pattern from seaweed to SB dendrite emerges when the pulling velocity is increased, which will not be discussed in this paper.

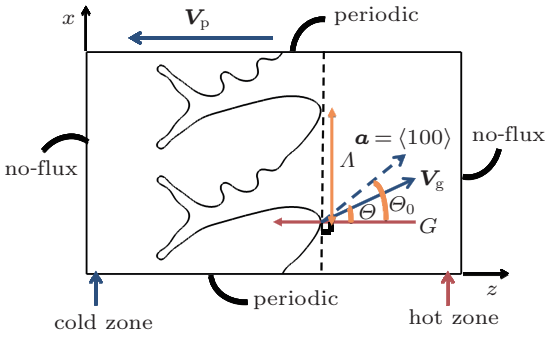


Fig. 1. (color online) Schematic diagram of the computational domain used in the numerical simulations of the dendrite to symmetry-broken fingers in directional solidification.

3. Results and discussion

We find that the morphological transition can be characterized by the characteristic angle Θ and the average primary dendritic spacing λ_1^*. For single tilted cells/dendrites, after the structure has reached the state stage, $\Theta\equiv\Theta_{\mathrm{tip}}$ can be calculated by

$$\Theta_{\mathrm{tip}}=\tan^{-1}\left(\left[x(t+\mathrm{d}t)-x(t)\right]/\left[y(t+\mathrm{d}t)-y(t)\right]\right). \qquad (12)$$

For the SB double dendrites, Θ is defined as the angle between the direction of the deep groove and the z axis using Eq. (12). Figure 2(a) shows Θ as a function of V_{p} with the typical interfacial morphologies corresponding to every state region, and the typical interfacial morphologies for the dendrite to SB dendrites transition when $\Theta_0=40°$. It can be seen from the insets that the interfacial morphology undergoes a transition from tilted cells/dendrites, to transition state fingers,

and to steady SB double dendrites with the increase of V_p. The transition state region can be divided into two sub-regions in the case of $\Theta_0 = 40^\circ$ according to the interfacial morphologies: a region of fine dendrites and a coexistence region of dendrites and SB double dendrites. Once V_p exceeds a certain critical value (around 13000 μm/s), the interfacial morphology transforms from SB double dendrites to unsteady fingers, where the resulting growth pattern cannot be spatially periodic because they are unsteady and chaotic. Also, the average primary dendritic spacing λ_1^* as a function of V_p is shown in Fig. 2(b). The morphological regions are separated and the insert shows the variation of Θ with Péclet number $Pe = V_p\lambda_1^*/D_l$, which satisfies the relation proposed by Deschamps *et al.*,[21]

$$\Theta = \Theta_0 - \Theta_0/(1 + aPe^b). \tag{13}$$

According to the variation of Θ, in the tilted dendrite/cell region, the real growth direction rotates from the z direction to the crystal orientation with the development of the side branches as Pe increases. Meanwhile, λ_1^* is nearly a constant. The results in the tilted cell/dendrits region can be fitted well by Eq. (13) with the fitting parameters $a = 0.12808$ and $b = 2.09482$. However, away from this region, the variation of Θ with Pe (V_p) no longer satisfies Eq. (13), and the increase of V_p results in a smooth decrease of Θ, as shown in Fig. 2(a). However, λ_1^* exhibits remarkable changes in different regions and sub-regions, and the value of λ_1^* is nearly unique at each region/sub-region. Thus, the evidence of the dendritic refinement and the dendrite to SB double dendrite transition can be quantified by examining the variation of λ_1^*. As shown in Fig. 2(b), λ_1^* decreases from 13.5 μm in the region of tilted dendrites/cells to 3.476 μm in the region of steady SB double dendrites as V_p increases. It is also observed that the width of the steady SB double dendrite region is rather narrow in comparison with that of other regions.

The overgrowth of the ternary arm is a common phenomenon to reduce the dendrite spacing, and the development of the tertiary arm exhibits a wide variety of growth patterns in the case of directional solidification of non-axially-oriented crystals. With the help of phase-field simulations, the growth of the ternary arm is quantitatively determined by the interdendritic undercooling by Wang *et al.*[28] In our simulations, we find that the mechanism of the transition from tilted dendrites/cells to subsequent complex structures can be explained by the development of ternary arms. The evolutions of three typical morphological ternary arms are shown in Fig. 3, i.e., fine dendrites in Figs. 3(a) and 3(b), SB double dendrites in Figs. 3(c) and 3(d), and SB multiple dendrites in Figs. 3(e) and 3(f). For the case of $\Theta_0 = 40^\circ$ and $V_p = 7500$ μm/s (Figs. 3(a) and 3(b)), each ternary arm on the secondary arms grows in an isolated mode, i.e., the pairs of the ternary arms separate with the primary spacing between the arms increasing gradually with time. Eventually, the primary spacing becomes nearly equivalent and fine dendrites form. Contrary to this case, the ternary arms grow with the neighboring arms in pair mode for the case of $\Theta_0 = 40^\circ$ and $V_p = 12000$ μm/s (Figs. 3(c) and 3(d)). This is because the increase of V_p provides more ternary arms, and the initial primary spacing between the periodic perturbations provides a larger space. Finally, the structure stabilizes in SB double dendrites, where two mirror dendrites are separated by a narrow groove of liquid of constant width, i.e., a stable width between two mirror dendrites. It indicates that if the distance between the arms falls within the stable range of the spacing of SB double dendrites, a pattern of SB double dendrites form, otherwise the dendritic structure appears. The SB multiple dendrites will be discussed later in the case of low Θ_0 and low V_p.

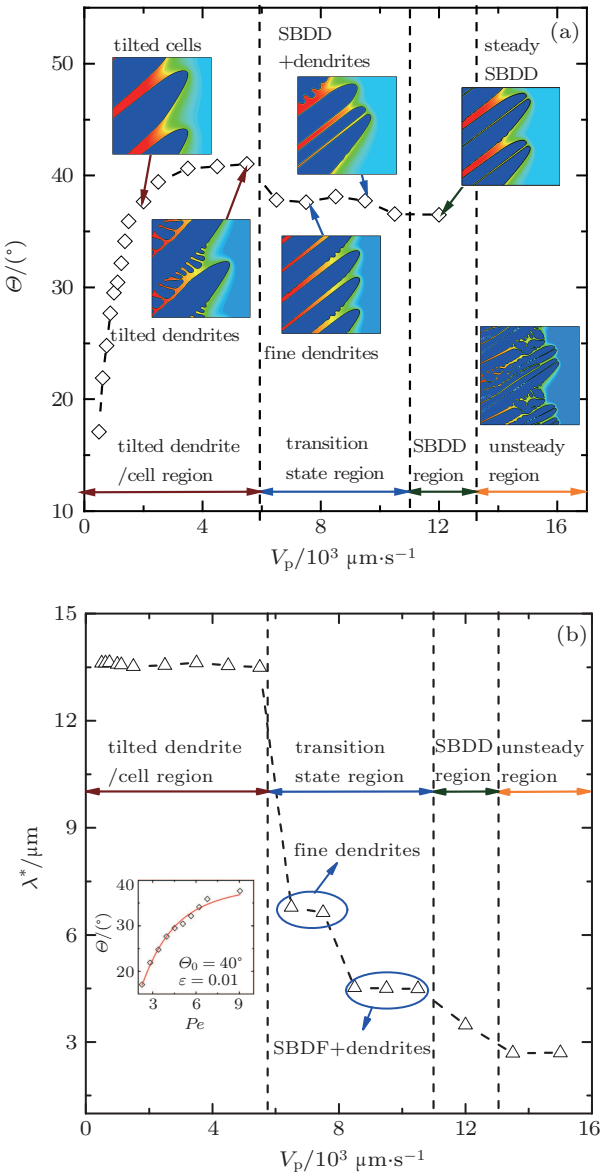
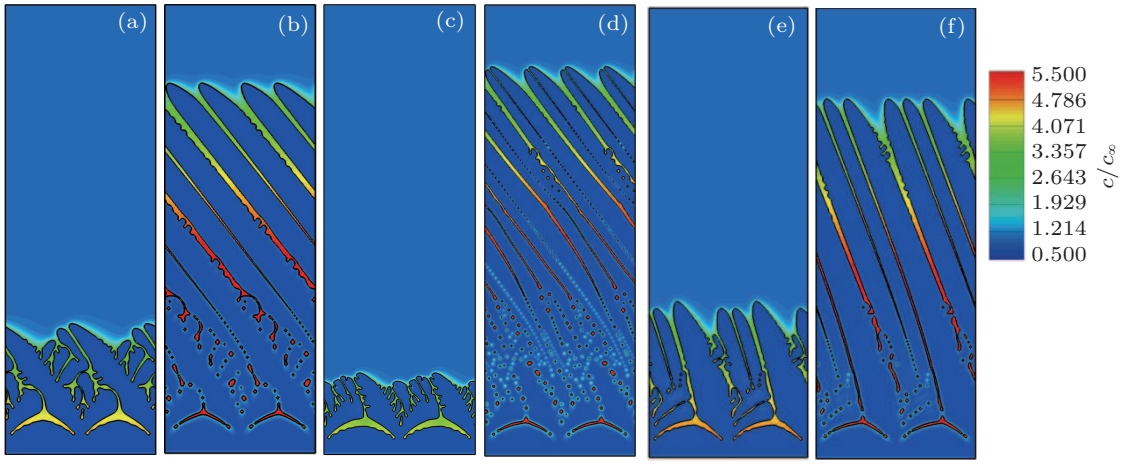


Fig. 2. (color online) (a) Characteristic angle Θ and (b) average dendritic spacing λ^* as a function of the pulling velocity V_p. Insets in panel (a) are the typical morphological growth patterns, and the inset in panel (b) is the Peclet number dependence of Θ.



Fiure 3. (color online) Morphological evolution of ternary arms for three typical cases: (a) and (b) $\Theta_0 = 40^\circ$ and $V_p = 7500$ μm/s; (c) and (d) $\Theta_0 = 40^\circ$ and $V_p = 12000$ μm/s; (e) and (f) $\Theta_0 = 20^\circ$ and $V_p = 10500$ μm/s.

In order to investigate the crystal orientation dependence of the growth pattern selections, phase-field simulations for different crystal orientations Θ_0 with variations of V_p are carried out. Figure 4(a) shows Θ as a function of V_p for different Θ_0. For all cases, Θ increases up to Θ_0 with the increase of V_p in the low pulling velocity range. Then it decreases slightly once V_p exceeds a certain critical value. It can be seen that the decrease of Θ_0 leads to the decrease of the critical velocity. However, the growth patterns are different for different Θ_0 with V_p increasing. Simulation results from all cases provide us with sufficient indications about the types of possible growth patterns in this problem. A morphological transition map for directional solidification of non-axially-oriented crystals is shown in Fig. 4(b). Four regions exist in this map: dendrite/cell region, transition state region, steady SB double dendrites region, and the unsteady region. The dendrite/cell region emerges at lower V_p, where Θ is a function of Pe, satisfying Eq. (13), as discussed above. The steady SB double dendrite region locates at the corner of the map, i.e., higher Θ_0 and higher V_p, while the unsteady state can be found when V_p is extremely large for a large Θ_0. Consequently, we can carefully propose that the final fate of the growth pattern is the unsteady state if V_p can be further increased. The transition region can be divided into three parts, where the intermediate states of growth patterns are included. The spacing of the dendrites is modified in the fine dendrite region, but from the point view of the interfacial morphology, it is very close to the tilted dendrite/cell. The SB multiple dendrite region occurs for lower Θ_0 and higher V_p where high-order symmetry-broken dendrites can be found. The typical interfacial morphology of the SB triple dendrites (a group of three dendrites) can be seen in the inset of Fig. 4(b), and Figs. 3(e) and 3(f) show the formation of SB triple dendrites at $\Theta_0 = 20^\circ$ and $V_p = 12000$ μm/s. It is clear that the SB triple dendrites have a typical sandwich structure, where an asymmetrical dendrite is sandwiched between two asymmetrical dendrites. Similarly to the SB double dendrites, the SB triple dendrites in simulations also result from the development of ternary arms. With the increase of V_p, SB multiple dendrites for lower Θ_0 and fine dendrites for higher Θ_0 can be converted into the intermediate state, a coexistence region of dendrites and SB double dendrites. It indicates that for higher V_p, the SB double dendrites are by far more preponderant than the other growth patterns. Therefore, we conjecture that the SB multiple dendrites can be considered as an intermediate growth pattern from tilted dendrites to SB double dendrites. In the experiments of SB double dendrite growth during directional solidification by Utter *et al.*,[22] an orientational dependence of the SB double dendrite growth was also observed, which is consistent with our results. We find that the SB double dendrites are oriented in particular directions, and the growth pattern selection depends strongly on the crystal orientations. Also, the direction of the SB double dendrites is a function of the crystal orientation (see Fig. 4(a) and the morphological map in Fig. 4(b)), which demonstrates that the stability and characters of the SB double dendrites are dependent on the crystal orientation. This implies that the anisotropy of the crystal forces the arrays of SB double dendrites to be close to the ⟨100⟩ axis. Similarly to the morphological diagrams in Refs. [11]–[13] and [16], the basis of higher velocity growth is the SB double dendrites in our simulations. However, there is no evidence that the SB double dendrites are the basis for seaweed growth if the unsteady pattern cannot be considered as the seaweed structure. With Θ_0 ranging from 15° to 40°, we find that the dendrites to symmetry-broken dendrites transition occurs with the increase of V_p. This transition could be considered as a process from a symmetrical state (arrays of dendrites) to a quasi-symmetrical state (arrays of pairwise fingers), where fine dendrites, the coexistence of SB double dendrites and dendrites, and SB multiple dendrites are seen as the transition states. Except for the unsteady state, we conjecture that the final fate of the growth pattern is the pattern with pairwise dendrites.

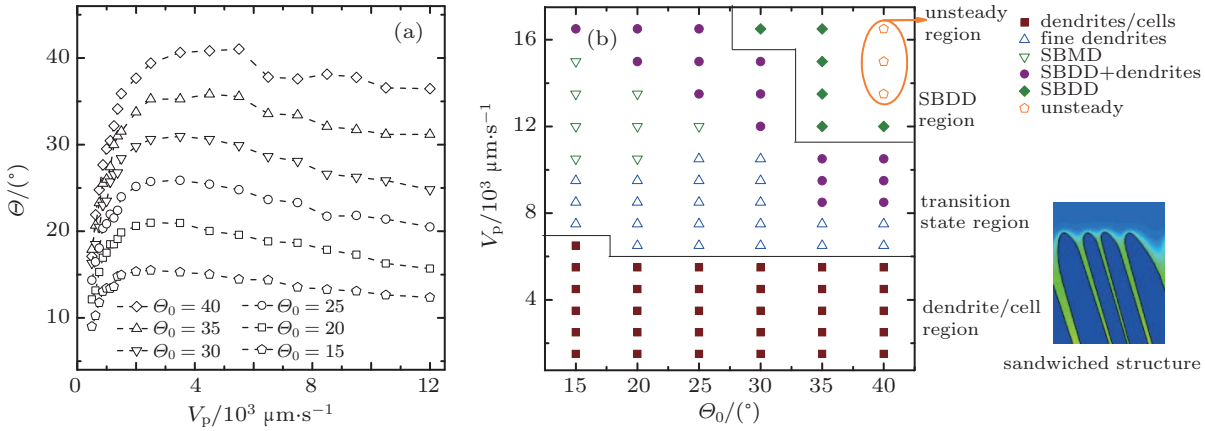


Fig. 4. (color online) (a) Characteristic angle Θ as a function of the pulling velocity V_p with different crystal orientation Θ_0. (b) Dendrites to symmetry-broken fingers transition map for the directional solidification of non-axially-oriented crystals.

4. Conclusion

In conclusion, the transition from dendrite to symmetry-broken double dendrites, existing in the directional solidification of non-axially-oriented crystals, can be characterized by the variation of the characteristic angle Θ and the average primary dendritic spacing λ^*. Specifically, we have discussed the morphology transition in the Θ_0–V_p space, in which the dendrite to symmetry-broken double dendrite transition emerges in the high V_p and high Θ_0 region. The SB double dendrites are oriented in particular directions with the growth pattern selection depending strongly on the crystal orientations. Although our simulations are carried out in two-dimensional space, the predicted results are useful to elucidate various aspects of the morphology transition during the directional solidification of non-axially oriented crystals. Also, three-dimensional simulations are needed for further investigations.

References

[1] Kurz W and Fisher D J 2001 *Fundamentals of Solidification* (4th edn.) (Enfield: Enfield Publishing and Distribution Company)
[2] Calliser W 2003 *Materials Science and Engineering an Introduction* (New York: Wiley)
[3] Haxhimali T, Karma A, Gonzales F and Rappaz M 2006 *Nature Mater.* **5** 660
[4] Salgado-Ordorica M A and Rappaz M 2008 *Acta Mater.* **56** 5708
[5] Amoorezaei M, Gurevich S and Provatas N 2010 *Acta Mater.* **58** 6115
[6] Mulins W W and Sekerka R F 1964 *J. Appl. Phys.* **35** 444
[7] Jamgotchian H, Trivedi R and Billia B 1993 *Phys. Rev. E* **47** 4313
[8] Kopczynski P, Karma A and Rappel W J 1997 *Phys. Rev. E* **55** 1282
[9] Losert W, Stillman D A, Cummins H Z, Kopczynski P, Rappel W J and Karma A 1998 *Phys. Rev. E* **58** 7492
[10] Akamatsu S, Faivre G and Ihle T 1995 *Phys. Rev. E* **51** 4751
[11] Ihle T and Muller-Krumbhaar H 1993 *Phys. Rev. Lett.* **70** 3083
[12] Ihle T and Muller-Krumbhaar H 1994 *Phys. Rev. E* **49** 2972
[13] Singer H M, Singer-Loginova I, Bilgram J H and Amberg G 2006 *J. Crystal Growth* **58** 296
[14] Kassner K, Valance A, Misbah C and Temkin D 1993 *Phys. Rev. E* **48** 1091
[15] Kupferman R, Kessler D and Ben-Jacob E 1995 *Physica A* **213** 451
[16] Ben Amnar M and Brener E 1995 *Phys. Rev. Lett.* **75** 561
[17] Georgelin M and Pocheau A 1997 *Phys. Rev. Lett.* **79** 2698
[18] Li J J, Wang J C and Wang G C 2008 *Chin. Phys. B* **17** 3516
[19] Akamatsu S and Ihle T 1997 *Phys. Rev. E* **56** 4479
[20] Pocheau A, Deschamps J and Georgelin M 2007 *JOM* **7** 71
[21] Deschamps J, Georgelin M and Pocheau A 2008 *Phys. Rev. E* **78** 011605
[22] Utter B and Bodenschaz E 2005 *Phys. Rev. E* **72** 011601
[23] Echebarria B, Folch R, Karma A and Plapp M 2004 *Phys. Rev. E* **70** 061604
[24] Wang Z J, Wang J C and Yang G C 2010 *Chin. Phys. B* **19** 078101
[25] Wang Z J, Wang J C and Yang G C 2010 *Chin. Phys. B* **19** 017305
[26] Shan L, Napolitano R E and Trivedi R 2001 *Acta Mater.* **49** 4271
[27] Badillo A and Beckermann C 2006 *Acta Mater.* **54** 2015
[28] Wang Z J, Li J J, Wang J C and Zhou Y H 2012 *Acta Mater.* **60** 1957